JOURNAL OF QUATERNARY SCIENCE (2022) **37**(2) 217–234 ISSN 0267-8179. DOI: 10.1002/jqs.3349

JQS Journal of Quaternary Science QRA Quaternary Research Association

Back to Uluzzo – archaeological, palaeoenvironmental and chronological context of the Mid–Upper Palaeolithic sequence at Uluzzo C Rock Shelter (Apulia, southern Italy)

E. E. SPINAPOLICE,[1]* A. ZERBONI,[2] M. C. MEYER,[3] S. TALAMO,[4,5] G. S. MARIANI,[6] L. A. GLIGANIC,[3] L. BUTI,[7] M. FUSCO,[1] M. P. MAIORANO,[8] S. SILVESTRINI,[7] R. SORRENTINO,[7,9] A. VAZZANA,[7] M. ROMANDINI,[7] A. FIORINI,[8] A. CURCI[8] and S. BENAZZI[5,7]

[1]Dipartimento di Scienze dell'Antichità, Sapienza Università di Roma, Roma, Italy
[2]Dipartimento di Scienze delle Terra 'A. Desio', Università Degli Studi di Milano, Milano, Italy
[3]Institute of Geology University of Innsbruck, Innsbruck, Austria
[4]Dipartimento di Chimica G. Ciamician, Università di Bologna, Bologna, Italy
[5]Department of Human Evolution, Max Planck Institute for Evolutionary Anthropology, Leipzig, Germany
[6]Dipartimento di Scienze Chimiche e Geologiche, Università Degli Studi di Cagliari, Cittadella Universitaria di Monserrato, Monserrato (CA), Italy
[7]Dipartimento di Beni Culturali, Università di Bologna, Ravenna, Italy
[8]Università di Bologna, Dipartimento di Storia Culture Civiltà, Bologna, Italy
[9]Department of Biological, Geological and Environmental Sciences – BiGeA, University of Bologna, Bologna, Italy

Received 15 October 2020; Revised 18 May 2021; Accepted 28 June 2021

ABSTRACT: The tempo and mode of *Homo sapiens* dispersal in Eurasia and the demise of Neanderthals has sparked debate about the dynamics of Neanderthal extinction and its relationship to the arrival of *H. sapiens*. In Italy, the so-called 'Transition' from Neanderthals to *H. sapiens* is related to the Uluzzian technocomplex, i.e. the first archaeological evidence for modern human dispersal on the European continent. This paper illustrates the new chronology and stratigraphy of Uluzzo C, a rock shelter and Uluzzian key site located in the Uluzzo Bay in southern Italy, where excavations are ongoing, refining the cultural sequence known from previous excavations. Microstratigraphic investigation suggests that most of the deposit formed after dismantling of the vault of the rock shelter and due to wind input of loess deflated by the continental shelf. The occasional reactivation of the hydrology of the local karst system under more humid conditions further contributed to the formation of specific layers accumulating former Terra Rossa-type soil fragments. Superposed on sedimentary processes, strong bioturbation and the mobilization and recrystallization of calcite have been detected. Optically stimulated luminescence (OSL) ages from Uluzzo C Rock Shelter are congruent with previously published radiocarbon ages obtained on shell beads and tephrachronology from adjacent sites preserving the Uluzzian technocomplex such as Grotta del Cavallo, confirming the onset for the Uluzzian in the area to ca. 39.2–42.0 ka. The OSL chronology from Uluzzo C also provides a terminus post quem for the end of the Mousterian in the region, constraining the disappearance of the Neanderthals in that part of Italy to $\geq 46 \pm 4$ ka.

KEYWORDS: Apulia; micromorphology; Neanderthal; OSL dating; Uluzzian; Uluzzo C Rock Shelter

Introduction

The Middle to Upper Palaeolithic (MP/UP) transition corresponds to the period between 50 and 40 ka BP, broadly identifying the time span when modern humans migrated into Europe and Neanderthals disappeared (Benazzi *et al.*, 2011, 2015, 2020; Douka *et al.*, 2014; Higham *et al.*, 2014; Fewlass *et al.*, 2020; Hublin *et al.*, 2020). Tracking the time and mode of the MP/UP transition is pivotal to understanding the biocultural processes that gave rise to the first major global replacement of populations and the establishment of humankind today, as indeed after 39 ka only modern humans inhabited Europe (Higham *et al.*, 2009, 2010, 2014; Benazzi *et al.*, 2011, 2015, 2020; Hublin, 2015; Fewlass *et al.*, 2020; Hublin *et al.*, 2020). Hence, there has been a resurgence of interest in the technological transitions observed in southern Europe in recent years (i.e. Italy and Greece; Higham *et al.*, 2009, 2014), and particularly for the Uluzzian, a lithic techno-complex associated with modern humans in the Italian peninsula, stratigraphically superposing the Mousterian, associated with Neanderthals (e.g. Benazzi *et al.*, 2011; d'Errico *et al.*, 2012; Moroni *et al.*, 2013; Marciani *et al.*, 2020). The taxonomic reassessment of modern human teeth retrieved from the Uluzzian deposit of Grotta del Cavallo (Benazzi *et al.*, 2011), coupled with a clarification of the stratigraphic sequence (Moroni *et al.*, 2018) and its geochronology (Douka *et al.*, 2014; Zanchetta *et al.*, 2018), makes the Uluzzian technocomplex a crucial element to unravel the biocultural processes that occurred during the MP/UP transition in Europe.

There are very few well-preserved and well-documented (in terms of stratigraphic coherence, chronological control and cultural evidence) archaeological sites preserving a stratigraphic sequence with Late Mousterian and Uluzzian assemblages and thus encompassing the MP/UP transition. In addition to Grotta del Cavallo, the most notable examples

*Correspondence: E. E. Spinapolice, as above.
E-mail: enzaelena.spinapolice@uniroma1.it

include Grotta Castelcivita (Moroni *et al.*, 2013), Grotta La Cala (Martini *et al.*, 2018), Grotta di Fumane and Riparo Broion (Peresani *et al.*, 2014, 2016, 2017, 2019), and Grotta Roccia San Sebastiano (Collina *et al.*, 2020). A further important sequence preserving the Late Mousterian to Uluzzian transition is the Carlo Cosma or Uluzzo C Rock Shelter, one of the sites where the Uluzzian technocomplex was defined. This site, located a few metres from Grotta del Cavallo (Fig. 1), was excavated in the1960s (Borzatti von Lowerstern, 1965, 1966; Borzatti von Löwerstern and Magaldi, 1966), and almost forgotten by the scientific community for about 50 years. This paper discusses preliminary results of the re-excavation at Uluzzo C Rock Shelter ongoing since 2016 (Fiorini *et al.*, 2018).

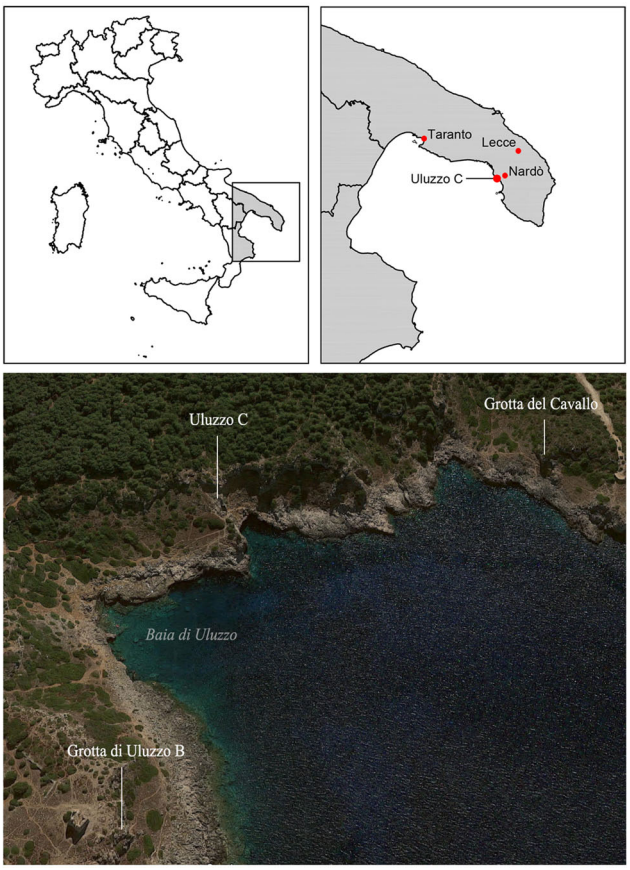

Figure 1. Maps illustrating the position of the Uluzzo C Rock Shelter in Italy and in Apulia; the oblique aerial view of the Uluzzo Bay indicates the positon of the nearby Grotta di Uluzzo B and Grotta del Cavallo sites. [Color figure can be viewed at wileyonlinelibrary.com]

The archaeological context

Uluzzo C Rock Shelter is located on the western side of the Apulian Coast (southern Italy), on the Ionian Sea (40°9′27.84″ N, 17°57′35.34″E). It lies in the middle of the Uluzzo Bay, south to Grotta di Uluzzo, located downstream of the Uluzzo Tower, in the Parco Naturale di Portoselvaggio (Nardò).

The site was discovered during archaeological investigations carried out by the Italian Institute of Prehistory and Protohistory (IIPP), led by Edoardo Borzatti von Löwerstern (Borzatti von Löwerstern, 1965, 1966; Borzatti von Löwerstern and Magaldi, 1966).

Uluzzo C Rock Shelter now appears as a central hall with a smaller cavity on its right side, characterized by the absence of archaeological deposits, probably washed-out by a recent reactivation of the karst hydrological network.

During its first exploration (1961–1966), the stratified deposit of the cave yielded rich lithic assemblages dating from the Mousterian to the Bronze Age, including the Uluzzian. Unfortunately, the upper levels, containing the signature of human presence in the Bronze Age, were destroyed by plunderers, and little archaeological sediments from that period have survived.

During the first excavations (1964–1966), a 2.6 × 1.5-m test trench was opened in the middle of the deposit, reaching a depth of 2.5 m. In 1966, the original trench was extended by 1 m^2, and at the end of the campaign, the bottom of the trench was about 8 m asl and had removed the central part of the deposit, identifying 22 spits within nine archaeologically distinct layers, labelled A to I by Borzatti von Löwerstern (Table 1).

According to Borzatti von Löwerstern and Magaldi (1966), layers H and I at the bottom of the deposit are analogous to the marine conglomerate identified a few metres from the cave made by large boulders perforated by lithodomes and covered by a conglomerate with small clasts. Moreover, Borzatti von Löwerstern and Magaldi (1966) suggested that the original

Table 1. Schematic archaeological sequence (modified after Borzatti von Löwerstern, 1965). According to Borzatti von Löwerstern (1965), layers η and σ are included in Layer G.

Layer	Depth	Cultural attribution	Description
A	0–17 cm	Romanellian	Sandy–silty layer formed by small discontinuous lenses and agglomerations of light-blue volcanic pumice sand and rare stones (α)
B	18–62 cm	Sterile	Volcanic sand, mixed with red quartz sandy grains; in the lower part grey pumice sandy layers (β)
C	63–80 cm	Uluzzian	Flowstone with rock debris from the dismantling of the roof of the rock shelter, covered by a sediment rich in manganese nodules and cemented by calcium carbonate
D	81–90 cm	Uluzzian	Looser and finer than Layer C
E	91–100 cm	Transition	Characterized by several concretions of red sandy soil covered up by a so-called 'purple volcanic soil' (δ) with few gravels
F	101–165 cm	Mousterian	Flowstone rich in gravel; Layer F is separated from Layer G by a thin level, σ
G	165–250 cm)	Mousterian	Loose dark-brown sediment consists of the upper part of medium–large rock fragments, rich in Mn oxy-hydroxide concretions; particularly rich in ash lenses and fireplaces. In the middle a layer with fewer rocks and oxidized (η)
H*	x	Mousterian	Red, deeply cemented sand layer at the top, a grey loose layer at its bottom, and a marine layer underneath the artificial cut 21 of the above layer G, with large calcareous pebbles (up to 1 m long) punctuated by lithodome perforations
I–L*	x	Mousterian	A conglomerate with smaller clasts in a sandy matrix, limestone and fossils of marine shells (*Ostrea* sp., *Nassa* sp., *Trochus* sp.) marks the underlying level that is clearly recognizable as an ancient beach

*Depth of Layers H–L are not given in the original publication.

floor of the cave corresponds to the last Marine Isotope Stage (MIS) 5e transgression event, based on the presence of several specimens of marine gastropods (e.g. *Strombus* sp.), at around 8–10 m asl. This constrains the age of the deposit having MIS 5e as a *terminus post quem*, as it happens for most of the Mousterian deposits of the region (Mastronuzzi and Sansò, 2002; Mastronuzzi *et al.*, 2007; Spinapolice, 2012, 2018a,b).

Materials and methods

The current investigation at Uluzzo C started in 2015 with a preliminary inspection, and the excavation began in 2016 (Fig. 2). This paper includes the geoarchaeological and geochronological data generated in the course of four excavation campaigns conducted between 2015 and 2018. Related archaeological materials are described in Silvestrini *et al.* (this volume).

The whole archaeological sequence has been sampled for optically stimulated luminescence (OSL) dating and sedimentological and microscopic analyses. Five OSL samples were obtained from the archaeological section, and sand-sized quartz grains (180–212 μm grain size) extracted using standard laboratory procedures (Wintle, 1997). Equivalent dose (*De*) values were obtained on the single-grain level using the single-aliquot regenerative-dose (SAR) protocol (Murray and Wintle, 2000) and appropriate quality assurance criteria applied to obtain single-grain *De* distributions (Murray and Wintle, 2000; Duller, 2003; Jacobs *et al.*, 2011). Dose rates were obtained via a combination of *in situ* gamma counting (Mercier and Falguères, 2007; Guérin and Mercier, 2011) and beta counting via a GM-25-5 low-level beta counter (Bøtter-Jensen and Mejdahl, 1988).

Figure 2. Excavations at Uluzzo C Rock Shelter 2016–2019; the area corresponds to squares AA9-11 and A9-11 in Fig. 3. Note the abundant vegetation before the onset of the new excavation. At the bottom of the picture is visible the trench of the old excavation. [Color figure can be viewed at wileyonlinelibrary.com]

The whole sequence was sampled for sedimentological (on bulk samples) and micromorphological (on undisturbed and orientated blocks) analyses. A detailed description of the methods used for excavation, geoarchaeological analyses, and dating is available in the Supporting Information (SI).

Results

Field evidence and investigated units

One of the major goals of the reappraisal at Uluzzo C was an updated understanding of the archaeological and sedimentological sequence (Figs. 2 and 3).

Layers A–C correspond to the Upper Palaeolithic and were almost completely removed by Borzatti von Löwernstern, except for the sediment leaning against the NW-facing wall (Fig. 4). Archaeologically, we do not have additional data from layers A–C, because we did not excavate them systematically. We decided not to remove these layers but leave them as evidence of the original cave filling, and for eventual future analyses, we exclusively sampled these layers for micromorphology and OSL dating.

Cleaning and analysis of the exposed stratigraphic section (Fig. 4) allowed us to identify the original archaeological layers left after Borzatti von Löwerstern's archaeological operations.

Thus, we have new data on the archaeological occupation in about half of the original surface of the rock shelter (for us Sector A) (Figs. 3 and 4), corresponding to Layer C of Borzatti von Löwerstern's stratigraphy at the beginning of our excavation.

Therein, we removed the uppermost (SU 6) and disturbed stratigraphic units (SU 16) contaminated with reworked sediment from the original excavation and bioturbated by recent vegetation (Fig. 2).

We stratigraphically excavated SU 3–19, which form the original Layer C, corresponding to the Final Uluzzian, while SUs 20–24 represent the beginning of Layer D and are under investigation. Nowadays, we consider layer D to be Uluzzian because of the characteristics of the lithics both from Borzatti von Löwerstern and our excavations (for details, see Silvestrini *et al.*, this volume). Most of the sequence is composed of $CaCO_3$-cemented layers; the exposed layers (C and D) also display the highest grade of cementation. The SUs investigated have a silty matrix and a reddish colour, are characterized by the abundance of faunal fragments (in some cases determinable; see also Silvestrini *et al.*, this volume) and Uluzzian lithic industry. In particular, several flint bladelets were found, confirming the bladelet production as characteristic of this 'modern' techno-complex (for details, see Silvestrini *et al.*, this volume). A variety of mammal species were identified, such as *Cervus elaphus* and carnivores such as *Vulpes vulpes* (Silvestrini *et al.*, this volume).

Sector B corresponds today to the bottom of the sequence excavated by Borzatti von Löwernstern. The stratigraphic section of Sector A is accessible via Sector B, and the geological and OSL samples of layers E to G (including the η and σ layers) were taken from this stratigraphic section (Fig. 5). Archaeologically, the G and η layers are known from former studies (Spinapolice, 2012, 2018a,b) as very dense occupation areas, with Mousterian technology and *in situ* fireplaces (Borzatti von Löwerstern and Magaldi, 1966).

Furthermore, the external area of the cave (Sector C, Fig. 4) was explored to test for the intact archaeological deposit. However, only reworked sediment from the old excavation was retrieved, lying directly on the bedrock.

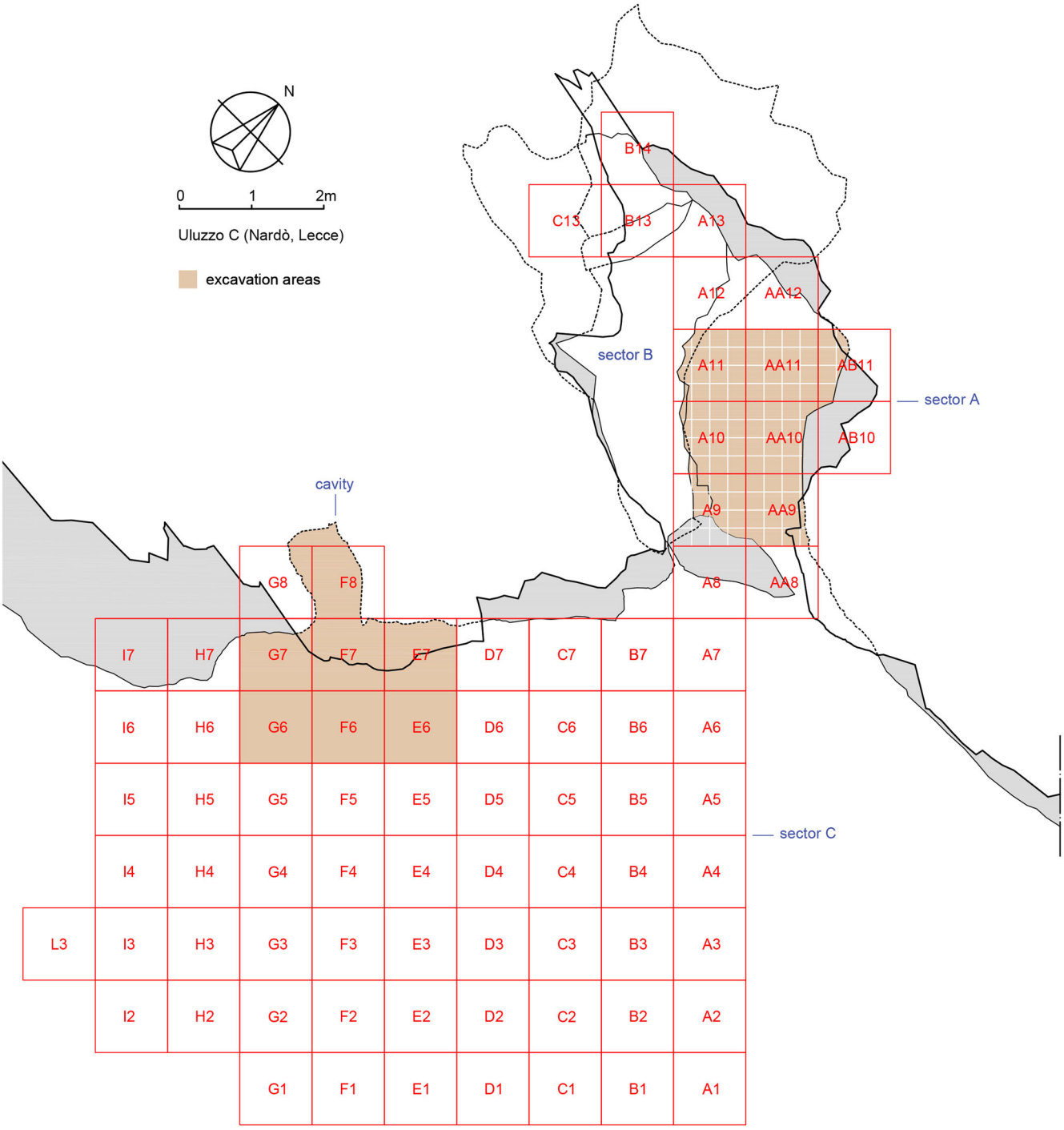

Figure 3. Map of the excavation areas. SECTOR A: excavation surface inside the shelter; SECTOR B: bottom of the previous excavation; SECTOR C: the area outside the cave. Excavation area in light brown. Dotted line: bottom of the rock shelter. Grey area: projecting wall. Continuous line: wall. [Color figure can be viewed at wileyonlinelibrary.com]

Geoarchaeological evidence

The sedimentary sequence

Exploration of the remnants of the stratigraphic sequence after the excavations of the 1960s almost confirmed the organization in SUs/Layers already described by Borzatti von Löwerstern and Magaldi (1966). The stratigraphic sequence here considered and described in Fig. 5 is what remains of previous excavations, and it is located in the innermost part of the rock shelter; layer labelling suggested by Borzatti von Lowerstern (1966) is adopted here for clarity.

The top of the stratigraphic sequence is sealed by a laminated, 10–20-cm-thick flowstone, probably formed during the Holocene. The uppermost part of the anthropogenic infilling of the rock shelter is Layer A, corresponding to a slightly reworked deposit. Layer A overlies a series of stratigraphic layers (B–F) bearing UP lithics, consisting of breccia-like layers with different amounts of fine matrix and in some cases displaying weak evidence of sedimentary structures. Layers B–F are cemented to moderately cemented by $CaCO_3$. Layer B is a weakly cemented, sand and silt matrix-supported breccia. Layer C is a cemented clast-supported breccia, with very little silty matrix, alternating laminae with common silty matrix; rock fragments are centimetre-sized and platy and accumulated according to weakly inclined bedding planes. The following Layer D is similar to Layer C, but the matrix is less abundant. Conversely, Layer E is a matrix-supported

Figure 4. Excavations at Uluzzo C. 2017 view of the site from the south; 2017 excavation of the Sector C (E–F–G 6–7); 2016 section against the NW wall (A12–AA12); 2018 excavation of Sector A (A10–11; AA10–11). [Color figure can be viewed at wileyonlinelibrary.com]

breccia, cemented by $CaCO_3$ and abundant silt; at the bottom of Layer E a thin layer of silt and fine sand is present. Layer F is again a clast-supported breccia with a silty to sandy matrix and interlayered by at least two thin layers of silt and fine sand. The amount of fine sediments increases towards the bottom of the layer, where large blocks from the collapse of the roof of the rock shelter are present. The transition to the lower part of the sequence – and the MP occupation of the site – is marked by an abrupt (erosive) transition between the bottom of the blocks of F and σ. The latter is a massive, moderately $CaCO_3$-cemented clay-rich matrix with some weakly rounded rock fragments. The following level η is a massive, silty to silty–clayey deposit interlayered by ash and charcoal-rich lenses; very few to common rock fragments are interspersed in the matrix along with charcoal fragments and centimetre-scale $CaCO_3$ nodules. The transition between η and G is an alignment of blocks collapsed from the roof of the rock shelter. Layer G is massive and moderately cemented, and silt and clay dominate the matrix, where very few rock fragments and $CaCO_3$ nodules are present. Occasionally, rock fragments form discontinuous alignments. According to Borzatti von Lowerstern (1966), these stratigraphic layers are in contact with an MIS 5e beach deposit, which actually is not evident along the sequence.

Sedimentological analyses

Chemical analyses on sediment samples showed mostly constant pH and total organic carbon (TOC) for the whole stratigraphic sequence (Table 2).

In particular, pH fluctuates around the mean value of around 8 by no more than 0.5 pH units. In absolute terms, the sediment is moderately alkaline, attributed to the high quantity of carbonates available in the environment and derived from the parent material and $CaCO_3$ recycling over time. TOC is always below 1% of the mass of the sediment.

Grain size analysis performed on the fine fraction of a selection of layers showed a general common trend in size distributions along the sequence. The main trend shows an abundance of fine sand and silt: silt notably represents between 40 and 60% of the total sediment. The finer portion of the sands are the second most represented group, with percentages ranging from 25 to 40%, while coarser fractions do not amount to more than 15% of the total. The least represented group is the finest: with the notable exception of layer σ, where it reaches 25%, clay never amounts to more than 10% on the total sediment. The graph of Fig. 6 shows two evident inflection points representing the main changes in relative abundance.

The first and clearest inflection point marks the steep increase at the passage from coarse to fine sand. The second, less pronounced, is located roughly around the shift from coarse to fine silt and shows a progressive decline of abundance towards clay. All investigated layers follow this model, with some minor exceptions. The most visible is in layer σ, which is shifted far more to finer material and shows a larger proportion of clay compared to silt, while sands remain similar to the general trend. On a smaller scale, layers ηb and Ga follow the opposite trend, where sand slightly increases while clay does not diverge. Layer B trends instead to a steeper curve, with a larger abundance of silts and a decrease in the sand and especially clay.

Micromorphology of thin sections

Essential micromorphological properties are summarized in the following parts and reported in Table 3, while the major observed features are illustrated in Fig. 7.

Layer A is composed of a heterogeneous yellowish-brown granular groundmass. It shows signs of transport from different sources based on the presence of subrounded quartz grains and rounded reddish pedorelicts originated from older and more developed soils. Bioturbation is evident around channel voids. Anthropogenic elements include bone, shell fragments and ash concentrations. The ash concentrations is often indistinguishable among the widespread calcite recrystallization pedofeatures, which in the upper part of the level form proper cementation, also associated with a general darker colour of the micromass. Unlike the previous Layer A, Layer C shows a higher degree of compaction, with a more coalescent groundmass and a blocky structure. However, the content is heterogeneous, with an increase in the frequency of quartz grains and bone fragments, while transported pedorelicts disappear. Signs of bioturbation are still evident. Microcharcoals – sometimes grouped in horizontal lines/lenses – and

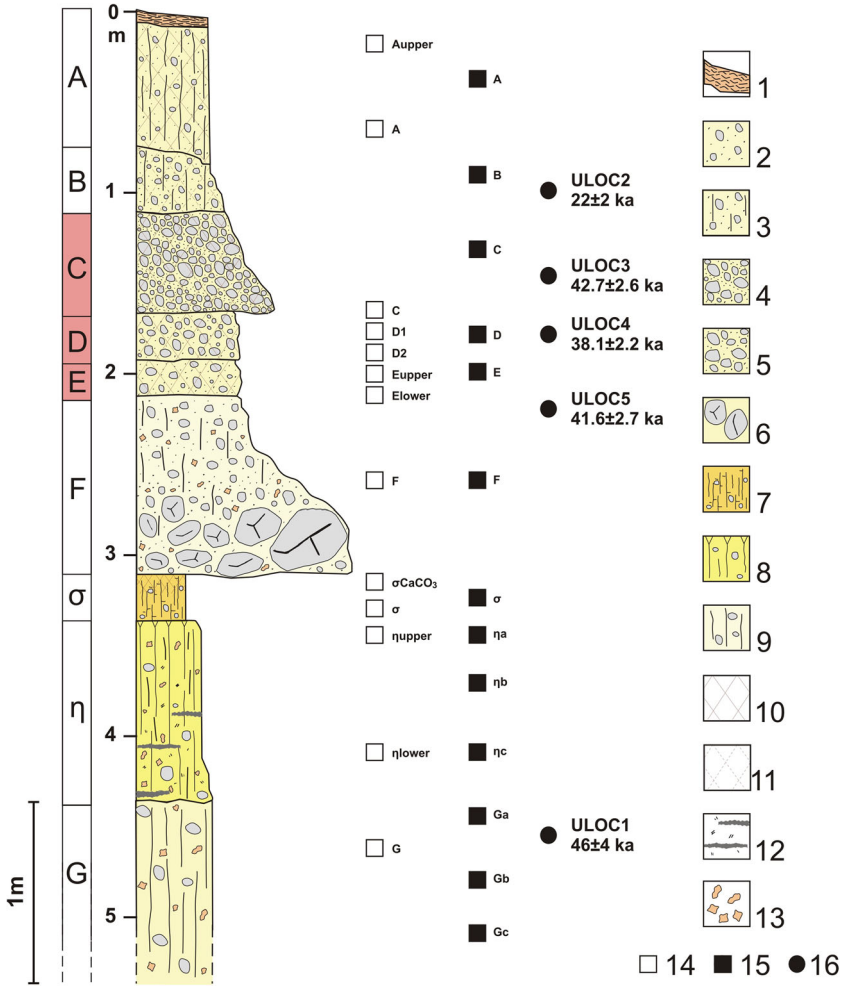

Figure 5. Stratigraphic log of the deposit of the Uluzzo C Rock Shelter indicating sampling points for sedimentological and micromorphological analyses and OSL dating; stratigraphic units are reported on the left. Key: (1) flowstone; (2) sandy unit with rock fragments; (3) sandy unit with rock fragments and bioturbation; (4) matrix- to clast-supported breccia displaying weak oblique lamination (sandy–silty matrix); (5) clast-supported breccia (sandy–silty matrix); (6) large blocks due to roof collapse; (7) clay-rich deposit with scarce rock fragments; (8) slightly weathered silty deposit with scarce rock fragments; (9) silty deposit with scarce rock fragments; (10) $CaCO_3$-cemented deposit; (11) weakly $CaCO_3$-cemented deposit; (12) charcoal fragments and ash-rich lenses; (13) $CaCO_3$ nodules and/or concretions; (14) sampling point for thin sections; (15) sampling point for sedimentological analyses; (16) sampling point for OSL dating. [Color figure can be viewed at wileyonlinelibrary.com]

Table 2. Summary of pH, TOC and grain-size (performed on poorly cemented deposits) analyses on samples from the stratigraphic sequence.

Stratigraphic unit	pH	TOC (g kg^{-1})	Gravel	Coarse sand	Medium sand	Fine sand	Silt	Clay
A	8.61	3.54	–	–	–	–	–	–
B	8.38	5.01	2.47	2.64	12.28	34.82	44.67	3.12
C	7.96	8.04	–	–	–	–	–	–
D	8.22	5.32	–	–	–	–	–	–
E	8.26	5.15	–	–	–	–	–	–
F	8.18	3.85	–	–	–	–	–	–
σ	8.24	2.81	11.34	6.38	5.85	18.80	32.27	25.36
η(a)	7.85	2.95	–	–	–	–	–	–
η(b)	8.35	4.43	19.71	7.95	7.30	21.68	35.89	7.47
η(c)	7.82	4.08	5.44	2.65	6.80	26.48	48.51	10.12
G(a)	7.73	4.13	15.18	6.35	13.58	18.24	35.96	10.69
G(b)	7.96	6.32	34.33	4.89	4.37	15.70	34.35	6.37
G(c)	7.93	5.50	13.20	3.37	5.47	19.44	51.30	6.86

phosphatic nodules appear. Calcite recrystallization is less common than in the upper part of the sequence.

Within Layer D, two different microfacies types can be recognized (D1 and D2). The first is mostly granular, less compacted and yellowish, with more evidence of bioturbation; it is composed of a more homogeneous groundmass with less ash and recrystallized calcite. D2 is darker and almost massive, with few horizontal voids, rich in bones and calcite cementation pedofeatures. Quartz grains and phosphate nodules are similar to Layer C. D1 and D2 microfacies types are chaotically distributed in the slide. Layer E is characterized by a homogeneous and massive dark microstructure, with widespread calcite cementation in the groundmass. Quartz grains, phosphatic nodules and bone fragments are similar to the upper levels; pedorelicts are absent. The bottom of the level changes considerably. Here, the microstructure is composed entirely of quartz grains and rounded pedorelicts with a more developed fabric than the ones found above. Bioturbation is absent, and other elements such as bone fragments, charcoal and phosphate nodules are rare; around these components, calcite infillings cement all the porosity. Calcite infillings remain dominant in Layer F, where $CaCO_3$ fills voids around the dark granules that make up the partially compacted groundmass effectively cementing the layer.

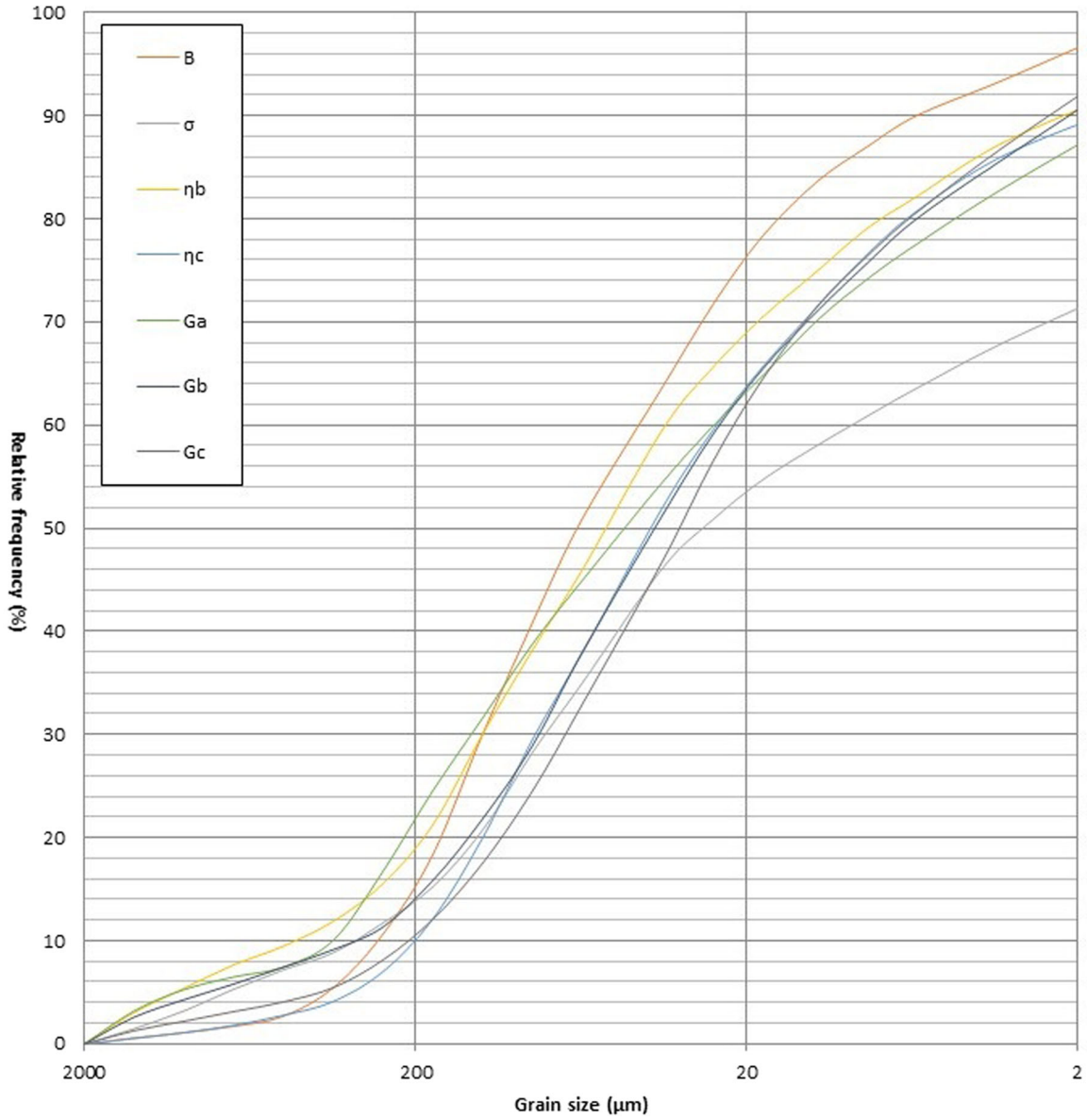

Figure 6. Cumulative grain size curves for selected layers from the Uluzzo C stratigraphic sequence (the *x*-axis is on a logarithmic scale). The distribution of most of the matrix of stratigraphic units overlaps the mean cumulative grain size curve of Italian loess elaborated by Cremaschi (1987). [Color figure can be viewed at wileyonlinelibrary.com]

Coarse components are less frequent: we noted a decrease in quartz grains, as well as pedorelicts (similar to those at the base of Layer E), bone fragments and ash accumulations. Below this level, all traces of bioturbation disappear.

The underlying Layer σ is blocky and more compacted, with brighter colour and very few voids. Quartz grains become frequent and show more variability in their dimensions than in the upper part of the sequence. Pedorelicts such as those above (Layers E and F) are very few, and sometimes weathered into Fe and Mn nodules. Dark amorphous organic material is locally present in the groundmass; frequent ash concentrations can also be found. Calcite recrystallization is limited compared to other layers, except for the cemented portions of the level, which are almost completely filled by calcite crystals.

Layer η shows similar features to σ. Except for the less massive microstructure, the other components are found in similar frequencies, including quartz fragments and amorphous organic material, which is replaced at its base by clusters of microcharcoals. Phosphate concentrations reappear here, both as nodules and as coatings around bone fragments. Calcite cementation progressively disappears downwards, where isolated concentrations of calcitic ash remain clearly visible. At the base of the level, several fragments of flint are present.

At the bottom of the section, Layer G is homogeneous and shows a dark granular microstructure inside dominant calcite crystals. The presence of other elements is limited to few fragments of quartz and rare bone and shell fragments, as well as pedorelicts similar to those above.

Geochronology

Optically stimulated luminescence dating

OSL dating was conducted on the single-grain level for all OSL samples (samples ULOC 1–5), and the corresponding equivalent dose (*De*) values and dose rates, as well as optical ages are summarized in Table 4 (compare SI for methodological details). Typical OSL decay curves for a bright and a dim grain in response to the natural and a regenerated dose are shown in Fig. 8. For both grains the OSL signals decay rapidly

Table 3. Summary of the main micromorphological properties of each stratigraphic unit.

Stratigraphic Unit	Micro-structure	Aggregates	Porosity	Mineral components	Organic components	Anthropo-genic components	c/f limit, ratio	c/f related distribution	Groundmass	b-fabric	Pedorelicts	Calcite	Phosphates	Passage features
A	Granular	Common to dominant mod. separated cemented granules CS to MS	Few complex packing voids MS to FS; few channels G to CS	Few well-sorted subrounded quartz grains FS to VFS; few mod. sorted subangular limestones G to CS	–	Few unburned/ burned bone fragments G to CS; rare shell fragments CS to FS; frequent ash deposits	10 µm, 20/80	Open fine enaulic	Yellowish brown, cloudy	Dark reddish brown, stipple speckled	Frequent rounded reddish and clayey pedorelicts G to MS	Dominant impregna-tive calcite coatings and hypo-coatings	–	Very few compaction hypocoat-ings around channels
A, upper part	Granular	Few mod. separated cemented granules CS to MS	Few complex packing voids MS to FS; few channels G to CS	Very few well-sorted subrounded quartz grains FS to VFS; few mod. sorted subangular limestones G to CS	–	Few unburned/ burned bone fragments G to CS; rare shell fragments CS to FS; frequent ash deposits	10 µm, 40/60	Double spaced fine enaulic	Brownish grey, cloudy	Dark reddish brown, stipple speckled	Very few rounded reddish and clayey pedorelicts CS to MS	Very dominant impregna-tive calcite coatings, infillings andHypo-coatings	–	Very few compaction hypocoat-ings around channels
C	Channel	Common to dominant mod. separated cemented granules CS to MS; few unseparated partially cemented subangular blocks G to VCS	Few complex packing voids MS to FS; few channels G to CS	Few well-sorted subrounded quartz grains VFS; few mod. sorted subangular limestones G to CS	–	Common unburned/ burned bone fragments G to CS; very few charcoals CS to FS; frequent ash deposits	10 µm, 20/80	Double spaced porphyric	Dark reddish brown, cloudy	Dark reddish brown, stipple speckled	–	Frequent impregna-tive calcite coatings and hypo-coatings	Rare subrounded phosphate nodules MS	Very few compaction hypocoat-ings around channels
D1	Channel	Dominant mod. separated cemented granules CS to MS; frequent unseparated	Few complex packing voids MS to FS; few channels G to CS	Few well-sorted subrounded quartz grains FS to VFS; few mod. sorted subangular	–	Few unburned/ burned bone fragments G to CS; frequent ash deposits	10 µm, 30/70	Double spaced porphyric	Yellowish brown, cloudy	Dark reddish brown, stipple speckled	–	Frequent impregna-tive calcite coatings and hypo-coatings	Rare subrounded phosphate nodules MS to FS	Very few compaction hypocoat-ings around channels

(*Continued*)

Table 3. (*Continued*)

Stratigraphic Unit	Micro-structure	Aggregates	Porosity	Mineral components	Organic components	Anthropo-genic components	c/f limit, ratio	c/f related distribution	Groundmass	b-fabric	Pedorelicts	Calcite	Phosphates	Passage features
		partially cemented subangular blocks G to VCS		limestones G to CS										
D2	Channel	Common mod. separated cemented granules CS to MS; dominant cemented subangular blocks G	Few complex packing voids MS to FS; few channels G to CS; very few horizontally orientated planar voids FS	Few well-sorted subrounded quartz grains FS to VFS; few mod. sorted subangular limestones G to CS	–	Common unburned/ burned bone fragments G to CS; dominant ash deposits	10 µm, 30/70	Double spaced porphyric	Dark reddish brown, cloudy	Dark brown, opaque	–	Common impregna-tive calcite coatings and hypo-coatings	Rare subrounded phosphate nodules MS to FS	Very few compaction hypocoat-ings around channels
E, upper part	Channel	Very dominant unseparated cemented subangular blocks G	Few to frequent channels VCS to MS	Few well-sorted subrounded quartz grains FS to VFS; very few mod. sorted subangular limestones G to CS	–	Very few unburned/ burned bone fragments G to CS; dominant ash deposits	10 µm, 30/70	Double spaced porphyric	Yellowish brown, locally dark reddish brown, cloudy	Dark reddish brown, stipple speckled, locally opaque	–	Common impregna-tive calcite coatings and hypo-coatings	Rare subrounded phosphate nodules MS to FS	Very few compaction hypocoat-ings around channels
E, lower part	Massive	–	Very few complex packing voids FS; few channels CS to MS	Frequent well-sorted subrounded quartz grains MS to VFS; few mod. sorted subrounded limestones G to VCS	–	Rare unburned/ burned bone fragments MS to FS; rare shell fragments MS to FS	10 µm, 70/30	Close porphyric	Brownish grey, cloudy	Grey, crystallitic	Common rounded orange brown clayey pedorelicts MS to FS; rare rounded microlami-nated fragmented limpid clay coatings FS	Dominant crystalline calcite coatings around coarse fragments	Rare subrounded phosphate nodules FS	–

(*Continued*)

Table 3. (*Continued*)

Stratigraphic Unit	Micro-structure	Aggregates	Porosity	Mineral components	Organic components	Anthropo-genic components	c/f limit, ratio	c/f related distribution	Groundmass	b-fabric	Pedorelicts	Calcite	Phosphates	Passage features
F	Channel	Dominant weak. separated cemented granules FS	Frequent channels VCS to CS	Very few well-sorted subrounded quartz grains MS to VFS; very few mod. sorted subrounded limestones G to VCS	–	Rare unburned/ burned bone fragments G to MS; rare shell fragments MS to FS; frequent ash deposits	10 µm, 35/65	Open fine enaulic	Dark brown, cloudy	Dark brown, crystallitic	Very few rounded orange brown clayey pedorelicts MS to FS	Dominant impregna-tive calcite coatings and hypo-coatings	–	Very few compaction hypocoat-ings around channels
σ CaCO3-cemented	Channel	Dominant weak. separated cemented subangular blocks VCS to MS	Few channels CS to MS; very few planar voids MS to VFS; rare vughs MS to FS	Frequent mod. sorted subrounded quartz grains FS to VFS; rare mod. sorted subrounded limestones G to VCS	–	Rare unburned/ burned bone fragments MS to FS	10 µm, 40/60	Single spaced porphyric	Yellowish brown, cloudy	Dark reddish brown, stipple speckled	Very few anorthic altero-morphic (from pedorelicts) rounded Fe-Mn nodules Ms to FS	Very dominant crystalline calcite coatings and infillings around coarse fragments	–	–
σ	Channel	Dominant weak. separated cemented subangular blocks G to VCS	Few channels CS to MS; very few planar voids MS to VFS	Frequent mod. sorted subrounded quartz grains FS to VFS; rare mod. sorted subrounded limestones G to VCS	Frequent amorphous organic fragments SM to SF	Rare unburned/ burned bone fragments MS to FS; locally frequent ash deposits	10 µm, 40/60	Single spaced porphyric	Yellowish brown, cloudy	Dark reddish brown, stipple speckled	Rare rounded orange brown clayey pedorelicts MS to FS; very few anorthic altero-morphic (from pedorelicts) rounded Fe-Mn nodules Ms to FS	Frequent crystalline calcite coatings and hypo-coatings	–	–
η, upper part	Channel	Very dominant weak. separated cemented subangular	Few channels CS to MS; very few planar voids MS to VFS; rare	Frequent well-sorted subrounded quartz grains FS to VFS; few	Few amorphous organic fragments SM to SF	Rare unburned/ burned bone fragments CS to FS;	10 µm, 30/70	Double spaced porphyric	Orangeish brown, cloudy	Dark reddish brown, stipple speckled	Very few rounded orange brown clayey pedorelicts	Locally few impregna-tive calcite coatings and hypo-	Few impregna-tive phosphate coatings around	–

(*Continued*)

Table 3. (*Continued*)

Stratigraphic Unit	Micro-structure	Aggregates	Porosity	Mineral components	Organic components	Anthropo-genic components	c/f limit, ratio	c/f related distribution	Groundmass	b-fabric	Pedorelicts	Calcite	Phosphates	Passage features
		blocks G to VCS; locally frequent mod. separated granules MS	vughs MS to FS	mod. sorted subrounded limestones G to VCS		locally frequent ash deposits					MS to FS; very few anorthic alteromorph-ic (from pedorelicts) rounded Fe-Mn nodules Ms to FS; rare rounded microlamina-ted fragmented limpid clay coatings FS	coatings	bones and locally coarse fragments; rare subrounded phosphate nodules FS	
η, lower part	Granular/ subangular blocky	Locally dominant mod. separated cemented subangular blocks G; locally dominant mod. separated granules VFS	Few channels CS to MS; very few complex packing voids VFS; rare planes FS to VFS	Frequent well-sorted subrounded quartz grains FS to VFS; rare mod. sorted subrounded limestones G to VCS	–	Few unburned/ burned bone fragments G to MS; rare clustered charcoals MS to FS; locally few ash deposits; rare flint fragments VCS	10 µm, 30/70	Double spaced porphyric	Orangeish brown, cloudy	Dark reddish brown, stipple speckled	Rare rounded orange brown clayey pedorelicts G to MS; very few anorthic altero-morphic (from pedorelicts) rounded Fe-Mn nodules Ms to FS	–	Rare subrounded phosphate nodules FS	–
G	Channel	Dominant well-separated cemented granules FS	Frequent channels VCS to CS	Very few well-sorted subrounded quartz grains MS to VFS; very few mod. sorted subrounded limestones CS to MS	–	Rare unburned/ burned bone fragments G to MS; rare shell fragments CS to FS; frequent ash deposits	10 µm, 45/55	Double spaced fine enaulic	Dark brown, cloudy	Dark brown, crystallitic	Very few rounded orange brown clayey pedorelicts VCS to FS	Dominant impregna-tive calcite coatings and hypo-coatings	–	–

Abbreviations: CS, coarse sand; FS, fine sand; G, gravel; MS, medium sand; VCS, very coarse sand; VFS, very fine sand.

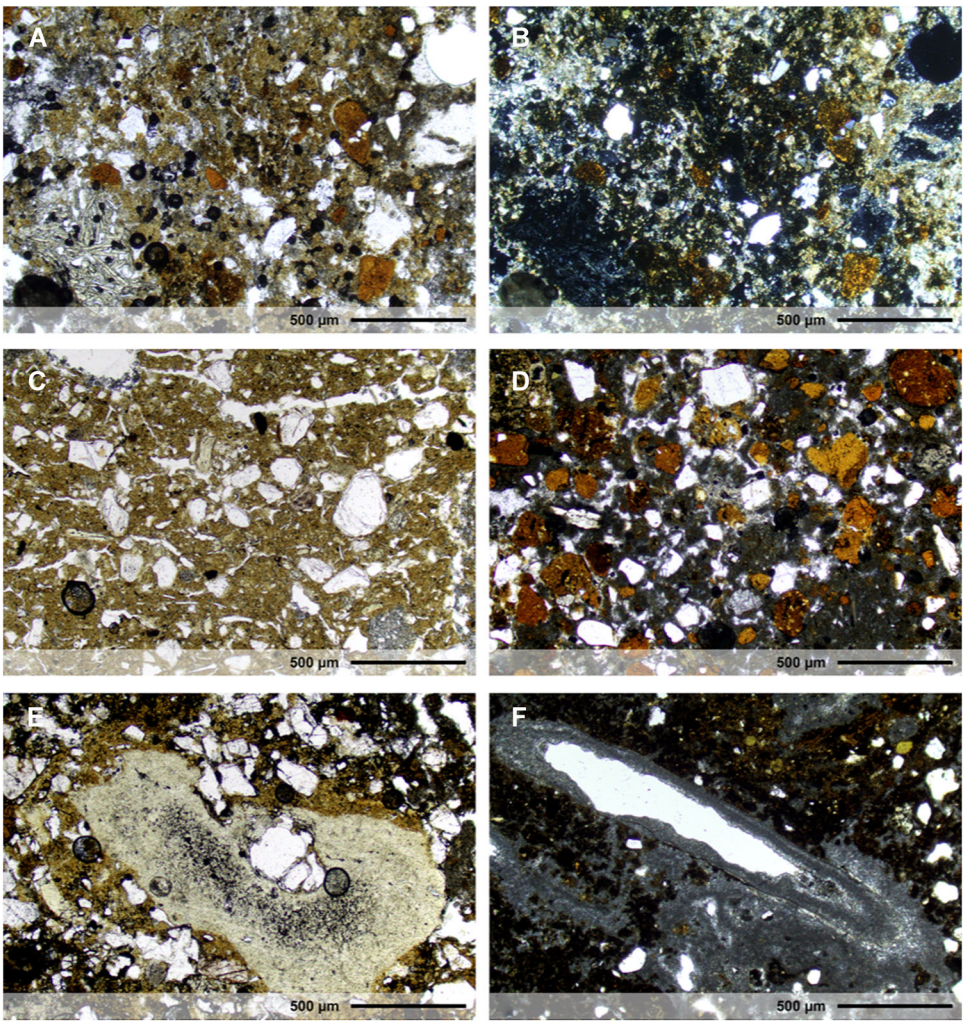

Figure 7. Micromorphological features of the studied levels: (A) reworked microstructure of Layer A, with rounded reddish pedorelicts and crystalline calcite filling the spaces between aggregates [plane polarized light (PPL)]; (B) same, in cross polarized light (XPL); (C) compacted massive microstructure in the matrix-supported portion of Layer D; note the horizontal alignments of voids and coarse mineral constituents possibly produced by trampling (PPL); (D) quartz grains and red rounded pedorelicts cemented by calcite at the base of Layer E (PPL); (E) phosphatization (in yellow) around a bone fragment in Layer η (PPL); (F) calcite recrystallization inside a channel in Layer G (PPL). [Color figure can be viewed at wileyonlinelibrary.com].

to background level within the initial ~0.5–1 s of stimulation time and the natural and regenerated OSL curves reveal similar shapes. These observations suggest that the quartz OSL signals are predominantly fast component-dominated, confirming that the SAR protocol is suitable for these samples (Wintle and Murray, 2006).

The overdispersion values (also σb values; Galbraith and Roberts, 2012) for samples ULOC 2–5 vary from 26 to 33% (Table 4) and *De* distributions are rather symmetrically distributed around the central weighted mean (Fig. 9 and SI), suggesting the presence of a single dose component. Indeed, σb values of ~20% have been commonly reported for 'ideal' (i.e. well-bleached and undisturbed) sedimentary quartz samples (e.g. Olley *et al.*, 2004; Arnold and Roberts, 2009). Hence, we opted for the central age model (CAM) to obtain an environmental burial dose for these samples (Galbraith *et al.*, 1999). The resulting optical ages for Uluzzian layers C, D and E (samples ULOC 3, 4 and 5) range from 38.1 ± 2.2 to 42.7 ± 2.6 ka (grand weighted mean 40.6 ± 1.4 ka). These three OSL ages have relative age uncertainties of 6% and overlap within error, thus constraining the timing of Uluzzian occupation of this rock shelter to MIS 3. The clustering of OSL ages for the Uluzzian layers also suggests that the duration of Uluzzian occupation of the site did not exceed a few millennia (eventually lasting from ca. 39 to 42 ka), and was potentially much shorter than that.

ULOC 1 (Mousterian layer G) has an optical age of 46 ± 4.0 ka and is in stratigraphic order. This OSL age must be interpreted as the minimum age for the Neanderthal presence and site occupation because we did not obtain additional OSL samples from deeper parts of the Mousterian complex.

Sample ULOC 2 (layer B) was a relatively loose sand deposit that was penetrated by rootlets at the time of sampling. This sample also showed a high overdispersion value (75.5%; Table 4), and a distinctive group of low *De* values can be seen in the corresponding radial plot (Fig. 9). This sedimentological observation in combination with the high overdispersion value of this sample suggests that this deposit and thus the single-grain *De* distribution is affected by younger intrusive grains that were worked in from above. The FMM (finite mixture model) was used to isolate this low *De* component from the main (i.e. high) *De* component (Roberts *et al.*, 1999; David *et al.*, 2007), for which an optical age of 22.4 ± 2 ka has been obtained (Table 4), and which is regarded as the depositional age for this sand deposit.

Table 4. Dose rates, number of measured and accepted grains, *De* values, age models, and resulting optical ages for the five OSL samples investigated in this study. CAM: central age model; FMM: finite mixture model. Note that for all OSL ages errors are reported at the 1-sigma level.

Samples (stratigraphic order)	Stratigraphic Layer	Water content (wt %)	Dose rate (Gy ka^{-1})		Number of grains				*De*(Gy) via CAM	SD	Over- dispersion (σ in %)	SD	Age model	Optical age (ka)	SD
			Total	SD	Measured (*n*)	Accepted (*n*)	Accepted %	Saturating (*n*)	Saturating (%)						
ULOC 2	B	18 ± 5	2.85	0.20	500	79	15.8	47	9.4	46.0	4.3	75.5	7.1	FMM	22.0	2.0
ULOC 3	C	5 ± 2.5	2.47	0.11	500	92	18.4	97	19.4	105.2	3.7	28.1	2.8	CAM	42.7	2.6
ULOC 4	D	5 ± 2.5	2.52	0.11	500	104	20.8	261	52.2	96.0	3.0	26.0	2.6	CAM	38.1	2.2
ULOC 5	E	5 ± 2.5	2.33	0.10	500	70	14.0	138	27.6	97.1	4.0	28.5	3.4	CAM	41.6	2.7
ULOC 1	G	18 ± 5	2.03	0.14	500	141	28.2	57	11.4	93.6	4.7	31.3	4.1	CAM	46.0	4.0

Radiocarbon dating

A single bone from US16 was pretreated at the Department of Human Evolution at the Max Planck Institute for Evolutionary Anthropology (MPI-EVA), Leipzig, Germany, and graphitized and dated at the Mannheim AMS laboratory (Lab Code MAMS) (Kromer *et al.*, 2013). The AMS ^{14}C result of the sample from US16 is 25 310 ± 77 ^{14}C BP (Table 5). In calibrated ages this date ranges from 29 820 to 29 320 cal BP at 68.2% probability and from 29 900 to 29 250 cal BP at 95.4% probability. The ^{14}C result was calibrated using IntCal20 in the OxCal v4.4 program (Bronk Ramsey, 2009; Reimer *et al.*, 2020). The result fits well with the structure of US16, characterized by soft silty–sandy brown sediment, associated with bioturbation, also testified by the presence of modern glass fragments noted during the excavation. The bone is also associated with shell and pottery fragments.

Discussion

One of the most notable results presented here is the revised version of the archaeological section that was originally been excavated and described in the 1960s. We were able to identify all the original archaeological layers and describe them in much finer detail (Fig. 5), and have provided the first numerical age control for this archaeological section, based on OSL dating (Table 4). The micromorphological analysis, together with high-resolution excavation methods, allowed us to understand both the origin of the deposit and the way human groups may have used this specific rock-shelter.

Field and analytical data suggest that the formation of the sequence is related to the accumulation of sediments via a range of depositional processes, mainly during MIS 3 to 2. As reported by Borzatti von Löwerstern and Magaldi (1966), the bottom of the sequence – not reached during our exploration – probably consists of MIS 5e beach deposits, which are quite common along the shores of the Italian Peninsula (Rovere *et al.*, 2016). Yet, the accessible part of the sequence (Layers A–G) was formed mostly by (i) the accumulation of sediments from the dismantling of the vault of the rock shelter due to spallation, (ii) the wind input of sediments probably deflated by the continental shelf that was subaerially exposed during MIS 4–2, (iii) the occasional reactivation of the hydrology of the local karst system and (iv) to a minor extent by human agency (anthropogenic debris). Superposed on the sedimentary processes, several post-depositional processes modified the deposits; among them, the most remarkable were bioturbation and the mobilization and recrystallization of calcite. Overall, the aeolian origin (Borzatti von Löwerstern and Magaldi, 1966) stated for most of the sediment is confirmed, and most of the layers show deposits with characteristics compatible with loess accumulation: the occurrence of allochthonous sub-rounded quartz grains detected in thin sections and the typical sigmoidal shape of cumulative grain-size curves (Fig. 6), dominated by the fine sand and silt fractions (see Cremaschi, 1987; Zerboni *et al.*, 2015). Moreover, windblown sediments originating from the shelf or the reworking of tephra are quite common in the region (Cremaschi and Ferraro, 2007; Hirniak *et al.*, 2020). As common in cave archaeological sites and considering sedimentological and micromorphological evidence, we can also consider humans as agents actively contributing to the accumulation of mineral grains and organic debris in the rock shelter (see Cremaschi *et al.*, 2014; MacPhail and Goldberg, 2018).

From a palaeoenvironmental point of view, the dismantling of the roof and walls of the rock shelter and the accumulation

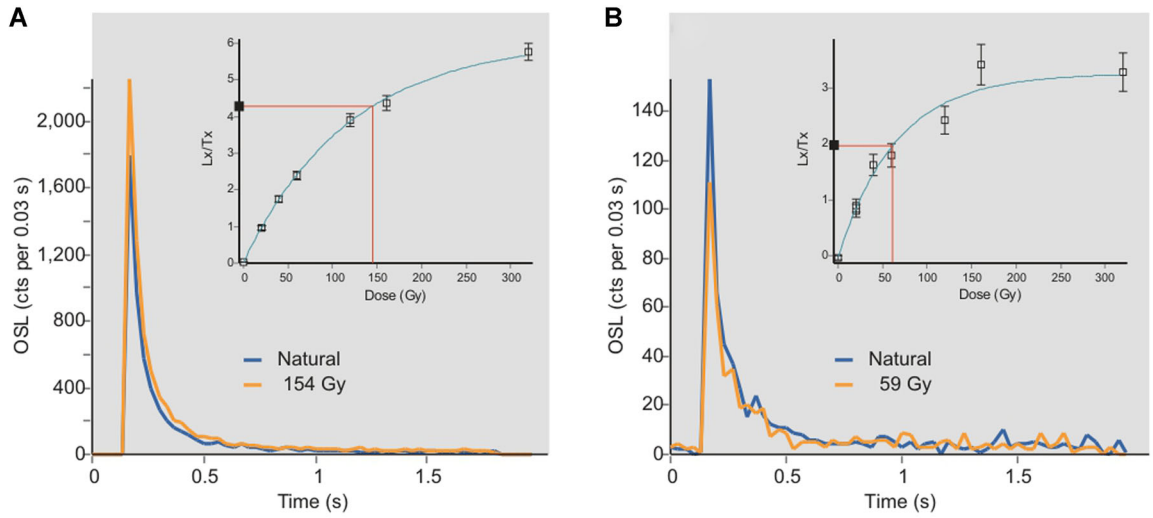

Figure 8. Typical OSL decay curves for a bright grain (A) and a dim grain (B) of sample ULOC 3. The decay curves of the natural signal (blue) and a regenerated signal (yellow) are plotted on top of each other. Inset shows corresponding dose–response curve fitted via an exponential function. [Color figure can be viewed at wileyonlinelibrary.com].

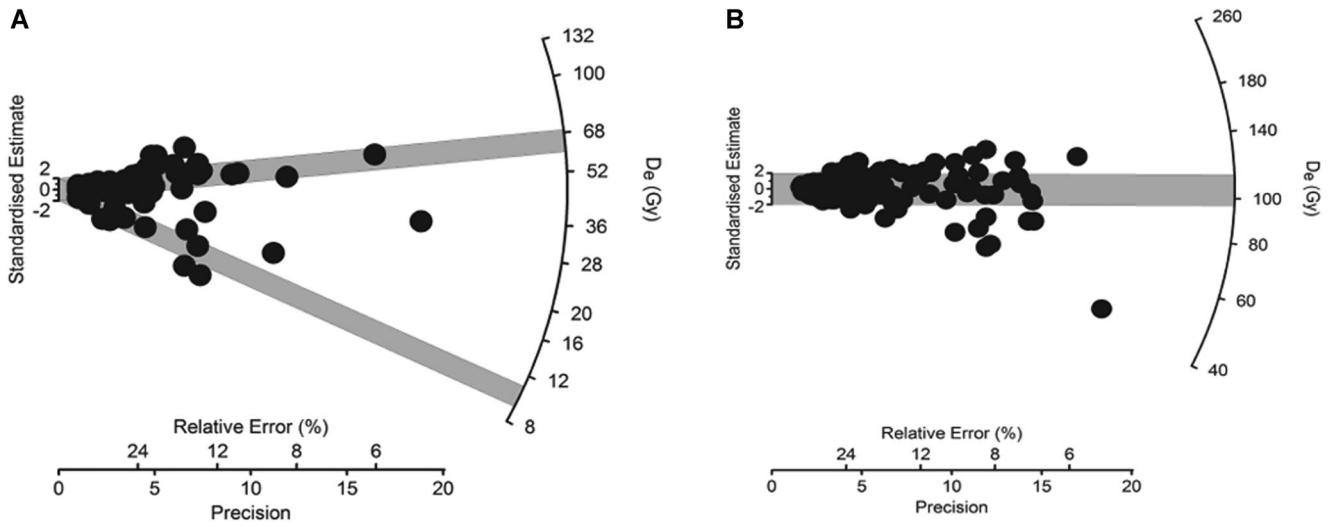

Figure 9. Radial plots of single-grain *De* distributions for selected OSL samples. A: sample ULOC 2 showing the two *De* components identified via finite mixture modelling (FMM). Grey bars indicate the 95% confidence interval for the low and high single-grain *De* populations, centred on ~10 and 64 Gy, respectively. B: sample ULOC 3 from the archaeological layer D. With the exception of one low *De* outlier with a *De* value of ~44 Gy, the single-grain *De* values are distributed rather symmetrically around a central weighted mean of ~105 Gy.

of windblown sediments are two sedimentary processes compatible with the cold and arid environmental conditions that prevailed during MIS 4 to 2 (Cremaschi and Ferraro, 2007; Hirniak *et al.*, 2020). Such conditions have been recently confirmed for southern Italy by rainfall reconstruction based on isotopic data from a speleothem that grew during the last glacial cycle in southern Apulia (Columbu *et al.*, 2020). Moreover, the breccia of layer C also suggests decreased temperatures and cooler environmental conditions at the time of deposition. The OSL ages of layer C–E overlap within error, yielding a grand weighted mean age for these Uluzzian layers of 40.6 ± 1.4 ka. This age thus also constrains the age of the breccia of layer C: it is thus likely that breccia deposition occurred during one of the stadial events (i.e. Greenland Stadial 9, 10 or 11; ca. 38.2–2.2 ka; NorthGrip Members, 2004; Rasmussen *et al.*, 2014). A more precise temporal correlation between this breccia deposit and cold climatic conditions recorded in the Greenland ice cores is not possible with current dating precision. The breccia deposit, in fact, has many analogies with the *grèzes litées* (*sensu* Ozouf *et al.*, 1995) and other frost-related coarse-grained deposits that form in rock shelters under glacial conditions (Laville *et al.*, 1980). We thus interpret Unit C as a *grèzes* litées-like deposit that probably accumulated via freezing–thawing cycles during a cool climatic phase.

Typical of the Uluzzo C Rock Shelter is the identification of the occasional accumulation of former soil fragments (pedorelict probably from cave infilling or Terra Rossa-type soils) in Layer E. Such pedorelicts formed after the occasional reactivation of the karst system, which was probably promoted by more humid conditions compatible with short interstadials or increased precipitation over the region. The speleothem record from Grotta Cucù Cave (Columbu *et al.*, 2020), for instance, suggests several short-term increases in rainfall during MIS 3; according to the chronology of the infilling of Uluzzo C, one of the wet phases preceding the H4 event (for instance at ca. 43 or 47 ka BP; Rasmussen *et al.*, 2014; Columbu *et al.*, 2020; Allard *et al.*, 2021) may have promoted

Table 5. Bone sample used for ^{14}C AMS dating. Isotopic value, C:N ratios, amount of collagen extracted (%Coll, >30-kDa fraction). The radiocarbon date is calibrated with IntCal20 using OxCal4.4. δ^{13}C values are reported relative to the vPDB standard, and δ^{15}N value is reported relative to the AIR standard.

MPI code	Submitter no.	Year	Square	Sector	U.S	Taxon	Collagen mass (mg)	Coll %	δ^{13}C	δ^{15}N	%C	%N	C:N	AMS code	^{14}C age	Err 1σ	Cal age BP 68.2%	Cal age BP 94.5%
R-EVA 3266	R204	2018	AA10	A	16	Ungulata	8	1.5	−19.52	7.8	37.63	14.08	3,12	ETH- 99095.1.1	25.310	77	29 820–29 320	29 900–29 250

the reactivation of the karst system. The Uluzzo C sequence is sealed by a flowstone covering highly bioturbated sediments. Bioturbation and precipitation of the flowstone occurred after the abandonment of the rock shelter and are compatible with Early Holocene wet environmental conditions (Columbu et al, 2020).

Furthermore, based on our high-resolution excavation methods, we obtained insights into the range of site activities.

The stratigraphic layers identified (C and D) correspond to occupation levels where an anthropogenic origin is predominant. Both knapping activities and activities linked to prey consumption and the exploitation of game and possibly marine resources are evidenced on site (see Silvestrini *et al.*, this volume). This is confirmed by the evidence of trampling in Layer D (regular horizontal void patterns and alignment of coarse mineral constituents, see Fig. 8), which we therefore interpret as a palaeosurface. The presence of microscopic bone fragments and phosphates possibly linked to the weathering of animal bones is coherent with the results from ancient DNA showing the occurrence of Cervidae and Equidae and the possible occasional presence of Hyenidae (Silvestrini *et al.*, 2021 this volume). These data together show an intense occupation in the rock shelter and a wide set of activities performed on site, at least for the time span corresponding to the Uluzzian occupation (Layers C and D). Unfortunately, the portion of the excavation removed in former test pits does not allow us to comment on the internal organization of the rock shelter during the Pleistocene. The shelter was possibly used a basecamp by one or more small bands during hunting or foraging who were undertaking subsistence activities as far as the sea (as attested by the presence of marine shells) and gathering lithic raw materials both locally and further away (Silvestrini *et al.*, this volume). The predominant presence of a recent Uluzzian at Uluzzo C is confirmed by technological analysis of the lithics (Silvestrini *et al.*, this volume); in fact, the schemes of the *chaînes operatoires*, having as a main goal the production of bladelets and flakelets, characteristic of the Uluzzian technocomplex (contra Mussi *et al.*, 2006; Zilhão *et al.*, 2015), strongly matches the European UP (Marciani *et al.*, 2020), and can be broadly compared with layer D of Grotta del Cavallo (Moroni *et al.*, 2018). Data from Uluzzo C thus confirm the Uluzzian as having fully modern behaviour expressed through techno-typologically complex lithic toolkits and highly adaptive subsistence strategies, a so-called 'Uluzzian package' (Douka *et al.*, 2014; Sano *et al.*, 2019; Arrighi *et al.*, 2020a,b,0c; Romandini *et al.*, 2020).

The OSL time constraints generated for the Uluzzian layers at Uluzzo C (i.e. a grand weighted mean OSL age of 40.6 ± 1.4 ka, calculated from the OSL ages of samples ULOC 3, 4 and 5) match the chronology of other Uluzzian sequences of the region, particularly the one from Grotta del Cavallo, which was – until now – the solely securely dated site in the region containing the Uluzzian technocomplex and human remains, marking a time frame for the arrival of modern humans in southern Italy. It has been suggested that during the ~55–48 ka phase of MIS 3 natural environments were favourable for *Homo sapiens* to enter Europe (Badino *et al.*, 2020; Hublin *et al.*, 2020), which is also in line with the earliest occurrences of *H. sapiens* in Turkey (Üçağızlı cave: Güleç *et al.*, 2002; Kuhn *et al.*, 2009), Lebanon (Ksar Akil: Copeland, and Yazbeck, 2002; Yazbeck, 2004; Douka *et al.*, 2013) and Israel (Manot Cave: Hershkovitz *et al.*, 2015).

Zanchetta *et al.* (2018) proposed a scenario for the human occupation of Apulia, based on the succession of tephra layers, and illustrated their hypothesis based on the correlation between regional human peopling and main climatic events, using Grotta del Cavallo as a reference site. At Uluzzo C, the

sequence lacks macroscopic tephra layers, and further analyses are required to examine whether cryptotephras, which were identified at other Mediterranean archaeological sites (Hirniak *et al.*, 2020), and are helpful in improving chronological precision, are present at Uluzzo C.

Zanchetta *et al.* (2018) note that the sedimentation rate at Grotta del Cavallo was highly variable, and comparably thick layers (e.g. Cavallo layer M) alternate with highly condensed ones (Cavallo D and E); this is probably the case at Uluzzo C. Despite the stratigraphic diversity, the chronological constraints for the end of the Mousterian in the area are overlapping for the two caves: 45.5 ± 1.0 ka at Grotta del Cavallo, and OSL-dated to 46 ± 4.0 ka at Uluzzo C (ULOC 1, Table 4). This fits with the accepted range for the disappearance of Neanderthals from the European continent, constrained to ca. 47–40 ka BP (e.g. Müller *et al.*, 2011; Hublin *et al.*, 2020).

Furthermore, Uluzzo C Rock Shelter, together with Grotta del Cavallo (Fabbri *et al.*, 2016) and Oscurusciuto (Boscato *et al.*, 2011), are now the only sites in southern Italy with secure time constraints for the presence of Neanderthals (see for a review Spinapolice, 2018a). Additional OSL sampling from the 2.5 m-thick Mousterian complex at Uluzzo C, from layer G, providing a minimum age of 46 ka gives further temporal insights into the MP and UP occupation history of the area.

At Uluzzo C the Uluzzian has been OSL dated to 39–42 ka (ULOC 3–5, Table 4), with 42 ka marking a *terminus post quem* for Uluzzian site occupation (i.e. 42 ka is the earliest possible date for occupation of the rock shelter by groups of modern humans). At Grotta del Cavallo, tephra stratigraphic investigation identified the Campanian Ignimbrite (CI) layer ($40^{Ar}/39^{Ar}$ dated at 39.850 ± 0.14 ka; Zanchetta *et al.*, 2018); this acts as a *terminus ante quem* for the Uluzzian occupation (i.e. modern humans were present no later than ca. 39.9 ka ago). Although Grotta del Cavallo and Uluzzo C are only a few tens of metres apart from each other, we have been unable to positively identify the CI at Uluzzo C. Zanchetta *et al.* (2018) suggest that the Uluzzian transitional complex in the region is constrained between ca. 46 and 39.9 ka. The grand weighted mean OSL age for the Uluzzian at the Rock Shelter Uluzzo C in combination with the numerically dated CI at Grotta del Cavallo allows us to refine the time window of the Uluzzian transitional complex and suggests that modern humans arrived in southern Italy some time between ca. 39.9 and 43 ka.

Yet, the current stratigraphic and geochronological resolution at both sites hampers us in constraining whether the Uluzzian persisted significantly beyond 39.9 ka, i.e. beyond the CI eruption.

The post-Uluzzian human occupation at Uluzzo C has been investigated by Borzatti von Löwenstern and is present at Grotta del Cavallo and Grotta di Uluzzo (Borzatti von Löwenstern, 1963, 1964; Palma di Cesnola, 1963, 1964). At Uluzzo C, Layer B, in the upper part of the sequence, has been OSL dated to the Last Glacial Maximum (ULOC2, 22.4 ± 2 ka, Table 4), and the radiocarbon date on a bone fragment from SU16 to $25\,310 \pm 77$ ^{14}C BP to the possible extent of the human occupation until MIS 3–2 will need further investigation. Disturbed Bronze Age evidence was also reported (Borzatti von Löwenstern, 1965), so possibly the occupation was interrupted in the Early Holocene and resumed only in the Late Holocene.

Conclusions

The arrival of *H. sapiens* in Europe and the demise of the Neanderthals are two potentially inter-related events that are hotly debated by the archaeological and palaeoanthropological community (e.g. Benazzi *et al.*, 2011; Higham *et al.*, 2011; Fewlass *et al.*, 2020; Hublin *et al.*, 2020). This debate is characterized by a wide range of assumptions, ranging from the idea of the relative inability of Neanderthals to survive competition with *H. sapiens* (e.g. Sano *et al.*, 2019), to an assumed cognitive comparability of *Homo neanderthalensis* with *H. sapiens* (e.g. d'Errico *et al.*, 1998; d'Errico and Banks, 2013, 2015).

Our new chronological, geoarchaeological and sedimentological data from Uluzzo C (i) constrain the Uluzzian at the Uluzzo C Rock Shelter to 39–42 ka, (ii) thus confirming the time span of the Uluzzian in southern Italy, and (iii) contribute the growing body of evidence suggesting an early arrival of modern humans in the southern Mediterranean. Collectively, our new data from Uluzzo C (see also Silvestrini *et al.*, this volume for analysis of lithic artefacts, faunal remains and ancient sedimentary DNA) provide us with more detailed insight into *H. sapiens* behaviour and organization of their technology and economy for a period when a crucial – yet little understood – population turnover occurred.

Supporting information

Additional supporting information can be found in the online version of this article.

Acknowledgements. We thank the Soprintendenza Archeologia, Belle Arti e Paesaggio per le Province di Brindisi, Lecce e Taranto for supporting our research in Uluzzo C Rock Shelter over the years, and particularly we thank Rino Bianco, Italo Muntoni and Serena Strafella. We are extremely grateful to Mino Natalizio (City Council), Vittorio Marras and the Gruppo Speleologico Neretino for all the logistic support during fieldwork. We are indebted to Lysann Rädisch, and Sven Steinbrenner of the Department of Human Evolution at the MPI-EVA for technical assistance. The radiocarbon date was supported by Max Planck Society. Research activities at Uluzzo C were mainly funded by the ERC no. 724046 – SUCCESS (http://www.erc-success.eu/) awarded to S.B. Fieldwork was also supported by the Leakey Foundation in the framework of the project Rediscovering the Uluzzian in Italy (2015/2016 general grant coordinated by M. Peresani). Geoarchaeological analyses were funded by Università degli Studi di Milano (Linea 2, 2016 and 2017 to A.Z.). Part of this research was supported by the Italian Ministry of Education, University, and Research (MIUR) through the project 'Dipartimenti di Eccellenza 2018–2022' (WP4 – Risorse del Patrimonio Culturale) awarded to the Dipartimento di Scienze della Terra 'A. Desio' of the Università degli Studi di Milano. E.E.S. was supported by the Rita Levi Montalcini 2013 programme.

Abbreviations. CAM, central age model; CI, Campanian Ignimbrite; FMM, finite mixture model; MIS, Marine Isotope Stage; MP/UP, Middle/Upper Palaeolithic; OSL, optically stimulated luminescence; SAR, single-aliquot regenerative-dose; SU, stratigraphic unit; TOC, total organic carbon.

References

Allard JL, Hughes PD, Woodward JC. 2021. Heinrich Stadial aridity forced Mediterranean-wide glacier retreat in the last cold stage. *Nature Geoscience* **14**: 197–205.

Arnold LJ, Roberts RG. 2009. Stochastic modelling of multi-grain equivalent dose (*De*) distributions: implications for OSL dating of sediment mixtures. *Quaternary Geochronology* **4**: 204–230.

Arrighi S, Bortolini E, Tassoni L *et al.* 2020a. Backdating systematic shell ornament making in Europe to 45,000 years ago. *Archaeological and Anthropological Sciences* **12**: 1–22.

Arrighi S, Marciani G, Rossini M *et al.* 2020c. Between the hammerstone and the anvil. Bipolar knapping and other percussive activities in the Late Mousterian and the Uluzzian of Grotta di Castelcivita (Italy). *Archaeological and Anthropological Sciences* **12**(1): 39.

Arrighi S, Moroni A, Tassoni L *et al*. 2020b. Bone tools, ornaments and other unusual objects during the Middle to Upper Palaeolithic transition in Italy. *Quaternary International* **551**: 169–187.
Badino F, Pini R, Ravazzi C *et al*. 2020. An overview of Alpine and Mediterranean palaeogeography, terrestrial ecosystems and climate history during MIS 3 with focus on the Middle to Upper Palaeolithic transition. *Quaternary International* **551**: 7–28.
Benazzi S, Arrighi S, Badino F *et al*. 2020. Peopling dynamics in the Mediterranean area between 45 and 39 ky ago: state of art and new data. *Quaternary International* **551**: 1–6.
Benazzi S, Douka K, Fornai C *et al*. 2011. Early dispersal of modern humans in Europe and implications for Neanderthal behaviour. *Nature* **479**: 525–528.
Benazzi S, Slon V, Talamo S *et al*. 2015. The makers of the Protoaurignacian and implications for Neandertal extinction. *Science* **348**: 793–796.
Borzatti von Löwenstern E. 1963. La Grotta di Uluzzo: campagna di scavi 1963. *Rivista di scienze preistoriche* **18**: 75–89.
Borzatti von Löwenstern E. 1964. La Grotta di Uluzzo: campagna di scavi 1964. *Rivista di scienze preistoriche* **19**: 41–52.
Borzatti von Löwerstern E. 1965. La Grotta- riparo di Uluzzo C. *Rivista di Scienze Preistoriche* **XX**: 1–31.
Borzatti von Lowerstern E. 1966. Alcuni aspetti del Musteriano del Salento. *Rivista di Scienze Preistoriche* **21**.
Borzatti von Löwerstern E, Magaldi D. 1966. Risultati conclusivi dello studio paletnologico e sedimentologico della Grotta di Uluzzo C (Nardò- Lecce). *Rivista di Scienze Preistoriche* **21**: 16–64.
Boscato P, Gambassini P, Ranaldo F *et al*. 2011. Management of Paleoenvironmental Resources and Raw materials Exploitation at the Middle Paleolithic Site of Oscurusciuto (Ginosa, Southern Italy): Units 1 and 4. In *Neanderthal Lifeways, Subsistence and Technology*, Conard NJ, Richter J (eds). Springer: Berlin; 87–98.
Bøtter-Jensen L, Mejdahl V. 1988. Assessment of beta dose-rate using a GM multicounter system. *International Journal of Radiation Applications and Instrumentation. Part D. Nuclear Tracks and Radiation Measurements* **14**: 187–191.
Bronk Ramsey C. 2009. Bayesian analysis of radiocarbon dates. *Radiocarbon* **51**: 337–360.
Collina C, Marciani G, Martini I *et al*. 2020. Refining the Uluzzian through a new lithic assemblage from Roccia San Sebastiano (Mondragone, southern Italy). *Quaternary International* **551**: 150–168.
Columbu A, Chiarini V, Spötl C *et al*. 2020. Speleothem record attests to stable environmental conditions during Neanderthal–modern human turnover in southern Italy. *Nature Ecology and Evolution* **4**: 1188–1195.
Copeland L, Yazbeck C. 2002. Inventory of Stone Age sites in Lebanon. Part III *Additions and Revisions, 1967–2001. Mélanges de l'Université Saint-Joseph* **55**: 119–325.
Cremaschi M. 1987. *Paleosols and Vetusols in the Central Po Plain (Northern Italy). A Study in Quaternary Geology and Soil Development*. Unicopli: Milan.
Cremaschi M, Ferraro F. 2007. The upper Pleistocene in the Paglicci Cave (Gargano, southern Italy): loess and tephra in the anthropogenic sequence. *Atti della Societa Toscana di Scienze Naturalie Memorie Serie A* **CXII** 153–163.
Cremaschi M, Zerboni A, Mercuri AM *et al*. 2014. Takarkori rock shelter (SW Libya): an archive of Holocene climate and environmental changes in the central Sahara. *Quaternary Science Reviews* **101**: 36–60.
d'Errico F, Banks WE. 2013. Identifying mechanisms behind middle Paleolithic and middle Stone Age cultural trajectories. *Current Anthropology* **54**: S371–S387.
d'Errico F, Banks WE. 2015. Tephra studies and the reconstruction of Middle-to-Upper Paleolithic cultural trajectories. *Quaternary Science Reviews* **118**: 182–193.
d'Errico F, Borgia V, Ronchitelli A. 2012. Uluzzian bone technology and its implications for the origin of behavioural modernity. *Quaternary International* **259**: 59–71.
d'Errico F, Zilhão J, Julien M *et al*. 1998. Neanderthal acculturation in western Europe? A critical review of the evidence and its interpretation. *Current Anthropology* **39**: S1–S44.
David B, Roberts RG, Magee J *et al*. 2007. Sediment mixing at Nonda Rock: investigations of stratigraphic integrity at an early archaeological site in northern Australia and implications for the human colonisation of the continent. *Journal of Quaternary Science* **22**: 449–479.
Douka K, Bergman CA, Hedges RE *et al*. 2013. Chronology of Ksar Akil (Lebanon) and implications for the colonization of Europe by anatomically modern humans. *PLoS ONE* **8**: e72931.
Douka K, Higham TF, Wood R *et al*. 2014. On the chronology of the Uluzzian. *Journal of Human Evolution* **68**: 1–13.
Duller GAT. 2003. Distinguishing quartz and feldspar in single grain luminescence measurements. *Radiation Measurements* **37**: 161–165.
Fabbri PF, Panetta D, Sarti L *et al*. 2016. Middle paleolithic human deciduous incisor from Grotta del Cavallo, Italy. *American Journal of Physical Anthropology* **161**: 506–512.
Fewlass H, Talamo S, Wacker L *et al*. 2020. A ^{14}C chronology for the Middle to Upper Palaeolithic transition at Bacho Kiro Cave. *Bulgaria. Nature Ecology and Evolution* **4**: 1.
Fiorini A, Curci A, Benazzi S *et al*. 2018. Il sistema di documentazione digitale dello scavo archeologico nel sito di Uluzzo C (Nardò, LE). *Sezione di Museologia Scientifica e Naturalistica* **13**: 68–70.
Galbraith RF, Roberts RG. 2012. Statistical aspects of equivalent dose and error calculation and display in OSL dating: an overview and some recommendations. *Quaternary Geochronology* **11**: 1–27.
Galbraith RF, Roberts RG, Laslett GM *et al*. 1999. Optical dating of single and multiple grains of quartz from Jinmium rock shelter, northern Australia: Part I, experimental design and statistical models. *Archaeometry* **41**: 339–364.
Guérin G, Mercier N. 2011. Determining gamma dose rates by field gamma spectroscopy in sedimentary media: results of Monte Carlo simulations. *Radiation Measurements* **46**: 190–195.
Güleç N, Hilton DR, Mutlu H. 2002. Helium isotope variations in Turkey: relationship to tectonics, volcanism and recent seismic activities. *Chemical Geology* **187**: 129–142.
Hershkovitz I, Marder O, Ayalon A *et al*. 2015. Levantine cranium from Manot Cave (Israel) foreshadows the first European modern humans. *Nature* **520**: 216–219.
Higham T, Brock F, Peresani M *et al*. 2009. Problems with radiocarbon dating the Middle to Upper Palaeolithic transition in Italy. *Quaternary Science Reviews* **28**: 1257–1267.
Higham T, Compton T, Stringer C *et al*. 2011. The earliest evidence for anatomically modern humans in northwestern Europe. *Nature* **479**: 521–524.
Higham T, Douka K, Wood R *et al*. 2014. The timing and spatiotemporal patterning of Neanderthal disappearance. *Nature* **512**: 306–309.
Higham T, Jacobi R, Julien M *et al*. 2010. Chronology of the Grotte du Renne (France) and implications for the context of ornaments and human remains within the Châtelperronian. *Proceedings of the National Academy of Sciences of the United States of America* **107**: 20234–20239.
Hirniak JN, Smith EI, Johnsen R *et al*. 2020. Discovery of cryptotephra at Middle–Upper Paleolithic sites Arma Veirana and Riparo Bombrini, Italy: a new link for broader geographic correlations, *Journal of Quaternary Science*. **35**: 199–212.
Hublin JJ. 2015. The modern human colonization of western Eurasia: when and where? *Quaternary Science Reviews* **118**: 194–210.
Hublin JJ, Sirakov N, Aldeias V *et al*. 2020. Initial upper Palaeolithic Homo sapiens from Bacho Kiro Cave, Bulgaria. *Nature* **581**: 299–302.
Jacobs Z, Meyer MC, Roberts RG *et al*. 2011. Single-grain OSL dating at la Grotte des Contrebandiers (Smugglers Cave), Morocco: improved age constraints for the Middle Paleolithic levels, *Journal of Archaeological Science* (**38**: 3631–3643.
Kromer B, Lindauer S, Synal HA *et al*. 2013. MAMS – A new AMS facility at the Curt-Engelhorn-Centre for Achaeometry, Mannheim, Germany. *Nuclear Instruments and Methods in Physics Research Section B* **294**: 11–13.
Kuhn SL, Stiner MC, Güleç E *et al*. 2009. The early upper paleolithic occupations at Üçağızlı cave (Hatay, Turkey). *Journal of Human Evolution* **56**: 87–113.
Laville H, Rigaud JP, Sackett J. 1980. *Rock Shelters of the Perigord: Geological Stratigraphy and Archaeological Succession*. Academic Press: Cambridge.
MacPhail RI, Goldberg P. 2018. *Applied Soils and Micromorphology in Archaeology*. Cambridge University Press: Cambridge.
Marciani G, Ronchitelli A, Arrighi S *et al*. 2020. Lithic technocomplexes in Italy from 50 to 39 thousand years BP: an overview of

lithic technological changes across the Middle-Upper Palaeolithic boundary. *Quaternary International* **551**: 123–149.

Martini I, Ronchitelli A, Arrighi S *et al*. 2018. Cave clastic sediments as a tool for refining the study of human occupation of prehistoric sites: insights from the cave site of la Cala (Cilento, southern Italy). *Journal of Quaternary Science* **33**: 586–596.

Mastronuzzi G, Quinif Y, Sansò P *et al*. 2007. Middle-Late Pleistocene polycyclic evolution of a stable coastal area (southern Apulia, Italy). *Geomorphology* **86**: 393–408.

Mastronuzzi G, Sansò P. 2002. Pleistocene sea-level changes, sapping processes and development of valley networks in the Apulia region (southern Italy). *Geomorphology* **46**: 19–34.

Mercier N, Falguères C. 2007. Field gamma dose-rate measurement with a NaI (Tl) detector: re-evaluation of the 'threshold' technique. *Ancient TL* **25**: 1–4.

Moroni A, Boscato P, Ronchitelli A. 2013. What roots for the Uluzzian? Modern behaviour in Central-Southern Italy and hypotheses on AMH dispersal routes. *Quaternary International* **316**: 27–44.

Moroni A, Ronchitelli A, Simona A *et al*. 2018. Grotta del cavallo (Apulia–Southern Italy). The uluzzian in the mirror. *Journal of Anthropological Sciences* **96**: 125–160.

Müller UC, Pross J, Tzedakis PC *et al*. 2011. The role of climate in the spread of modern humans into Europe. *Quaternary Science Reviews* **30**: 273–279.

Murray AS, Wintle AG. 2000. Luminescence dating of quartz using an improved single-aliquot regenerative-dose protocol. *Radiation Measurements* **32**: 57–73.

Mussi M, Gioia P, Negrino F. 2006. Ten small sites: the diversity of the Italian Aurignacian. In *Towards a Definition of the Aurignacian*, Bar-Yosef O, Zilhao J (eds). American School of Prehistoric Research/ Instituto Português de Arqueologia: Lisboa.

North Greenland Ice-Core Project (NorthGRIP) Members (2004). High resolution climate record of the Northern Hemisphere reaching into the last Glacial Interglacial Period. *Nature* **431**:147–151.

Olley JM, De Deckker P, Roberts RG *et al*. 2004. Optical dating of deep-sea sediments using single grains of quartz: a comparison with radiocarbon. *Sedimentary Geology* **169**: 175–189.

Ozouf J-C, Texier J-P, Bertran P *et al*. 1995. Quelques Coupes Caractéristiques dans les Départments de Versant d'Aquitaine Septentrionale: fades et Interprétation Dynamique. *Permafrost and Periglacial Processes* **6**: 89–101.

Palma di Cesnola A. 1963. Prima campagna di scavi nella Grotta del Cavallo presso Santa Caterina (Lecce). *Rivista di Scienze Preistoriche* **18**: 41–74.

Palma di Cesnola A. 1964. Seconda campagna di scavi nella Grotta del Cavallo presso Santa Caterina (Lecce). *Rivista di Scienze Preistoriche* **19**: 23–39.

Peresani M, Romandini M, Duches R *et al*. 2014. New evidence for the Mousterian and Gravettian at Rio Secco Cave, Italy. *Journal of Field Archaeology* **39/4**: 401–416.

Peresani M, Bertola S, Delpiano D *et al*. 2019. The Uluzzian in the north of Italy: insights around the new evidence at Riparo Broion. *Archaeological and Anthropological Sciences* **11**: 3503–3536.

Peresani M, Cristiani E, Romandini M. 2016. The Uluzzian technology of Grotta di Fumane and its implication for reconstructing cultural dynamics in the Middle-Upper Palaeolithic transition of western Eurasia. *Journal of Human Evolution* **91**: 36–56.

Peresani M, Delpiano D, Romandini M. 2017. Uluzzian vs Uluzzian: implications of a new site discovered in the north of Italy. In 7th Annual Meeting of the European Society for the Study of Human Evolution. *European Society for the study of Human Evolution*: 144–144.

Rasmussen SO, Bigler M, Blockley SP *et al*. 2014. A stratigraphic framework for abrupt climatic changes during the Last Glacial period based on three synchronized Greenland ice-core records: refining and extending the INTIMATE event stratigraphy. *Quaternary Science Reviews* **106**: 14–28.

Reimer PJ, Austin WEN, Bard E *et al*. 2020. The IntCal20 Northern Hemisphere radiocarbon age calibration curve (0–55 cal kBP). *Radiocarbon* **62**: 725–757.

Roberts RG, Galbraith RF, Olley JM *et al*. 1999. Optical dating of single and multiple grains of quartz from Jinmium rock shelter, northern Australia: Part II, results and implications. *Archaeometry* **41**: 365–395.

Romandini M, Crezzini J, Bortolini E *et al*. 2020. Macromammal and bird assemblages across the Late Middle to Upper Palaeolithic transition in Italy: an extended zooarchaeological review. *Quaternary International* **551**: 188–223.

Rovere A, Raymo ME, Vacchi M *et al*. 2016. The analysis of Last Interglacial (MIS 5e) relative sea-level indicators: reconstructing sea-level in a warmer world. *Earth-Science Reviews* **159**: 404–427.

Sano K, Arrighi S, Stani C *et al*. 2019. The earliest evidence for mechanically delivered projectile weapons in Europe. *Nature Ecology and Evolution* **3**: 1409–1414.

Spinapolice EE. 2012. Raw material economy in Salento (Apulia, Italy): new perspectives on Neanderthal mobility patterns. *Journal of Archaeological Science* **39**: 680–689.

Spinapolice EE. 2018a. *Les Néandertaliens du talon Technologie lithique et mobilité au Paléolithique moyen dans le Salento (Pouilles, Italie méridionale)*. Archaeopress: Oxford.

Spinapolice EE. 2018b. Neanderthal mobility pattern and technological organization in the Salento (Apulia, Italy). In *Palaeolithic Italy Advanced Studies on Early Human Adaptations in the Apennine Peninsula*, Sidestone Press Acadmics: Leiden; 95–124.

Wintle AG. 1997. Luminescence dating: laboratory procedures and protocols. *Radiation Measurements* **27**: 769–817.

Wintle AG, Murray AS. 2006. A review of quartz optically stimulated luminescence characteristics and their relevance in single-aliquot regeneration dating protocols. *Radiation Measurements* **41**: 369–391.

Yazbeck C. 2004. Le Paléolithique du Liban: bilan critique. *Paléorient* **30**: 111–126.

Zanchetta G, Giaccio B, Bini M *et al*. 2018. Tephrostratigraphy of Grotta del Cavallo, Southern Italy: insights on the chronology of Middle to Upper Palaeolithic transition in the Mediterranean. *Quaternary Science Reviews* **182**: 65–77.

Zerboni A, Trombino L, Frigerio C *et al*. 2015. The loess-paleosol sequence at Monte Netto: a record of climate change in the Upper Pleistocene of the central Po Plain, northern Italy. *Journal of Soils and Sediments* **15**: 1329–1350.

Zilhão J, Banks WE, d'Errico F *et al*. 2015. Analysis of site formation and assemblage integrity does not support attribution of the Uluzzian to modern humans at Grotta del Cavallo. *PLoS ONE* **10**: e0131181.

